NUCL SCI TECH (2020) 31:14
https://doi.org/10.1007/s41365-020-0727-7

Contributions of optimized tensor interactions on the binding energies of nuclei

Di Wu[1] · Chun-Lin Bai[1] · H. Sagawa[2,3] · Zeng-Qiang Song[1] · Huan-Qiao Zhang[4]

Received: 15 October 2019 / Revised: 12 November 2019 / Accepted: 3 December 2019 / Published online: 28 January 2020

Abstract The tensor parts of Skyrme interactions are constrained from the collective charge-exchange spin–dipole and Gamow–Teller excitation energies in ^{90}Zr and ^{208}Pb, together with the isotopic dependence of energy splitting between proton $h_{11/2}$ and $g_{7/2}$ single-particle orbits along the $Z = 50$ isotopes. With the optimized tensor interactions, the binding energies of spherical or weakly deformed nuclei with $A = 54-228$ are studied systematically. The present results show that the global effect of tensor interaction is attractive and systematically increases the binding energies of all these nuclei and makes the nuclei more bound. The root mean squared deviation of the calculated binding energies from the experimental values is significantly improved by the optimized tensor interactions, and the contribution of the tensor interaction to the binding energy is estimated.

Keywords Tensor force · Binding energy · Gamow–Teller transition · Spin–dipole transition · Single-particle energy differences

This work is supported by the National Natural Science Foundation of China (Nos. 11575120 and 11822504) and JSPS KAKENHI (No. JP19K03858).

✉ Chun-Lin Bai
bclphy@scu.edu.cn

[1] College of Physics, Sichuan University, Chengdu 610065, China

[2] RIKEN Nishina Center, Wako 351-0198, Japan

[3] Center for Mathematics and Physics, University of Aizu, Aizu-Wakamatsu, Fukushima 965-8560, Japan

[4] China Institute of Atomic Energy, Beijing 102413, China

1 Introduction

Nuclear energy density functionals (EDFs) such as Skyrme, Gogny, and relativistic mean field models (RMF, RHF) have achieved great success for describing the properties of nuclear ground states as well as excited states in the last few decades [1–4]. By fitting to a set of experimental data, primarily saturation properties of nuclear matter, binding energies, and charge radii of some closed shell nuclei, EDFs can predict the properties of ground states and excited state, i.e., excitation energies and transition strengths of both low-lying collective states and giant resonances along the wide region of nuclear chart.

Tensor force is an important component of the bare nucleon–nucleon interaction [5]; specifically, it was recognized historically as an essential constituent to make the deuteron bound [6]. However, its relevance for EDF has been discarded for a long time after the early achievement of Skyrme interactions in the 1970s. This implies that in earlier implementations of density functional theory (DFT), based on effective interactions such as Skyrme's, the tensor force was either considered of trivial importance or ignored for the purpose of simplicity. Diversely, the Skyrme EDFs show explicit contributions of tensor interactions. The contributions are demonstrated in the spin–orbit potential as the spin–current density with those from the momentum-dependent terms of the central force. As these terms vanish in spin–orbit saturated nuclei, and many nuclei used in the fits belong to these nuclei, most of the early Skyrme parametrizations ignored not only the tensor terms but also the spin–current terms [7].

The revival of tensor terms occurred in the beginning of the twenty-first century with the development of new radioactive ion beam facilities, by which more neutron-rich

nuclei have been studied and new phenomena have been observed with respect to the evolution of the spin–orbit splitting with neutron excess [8]. Afterward, the importance of an effective neutron–proton tensor force was suggested to explain this evolution [9]. Inclusion of tensor terms could produce more qualitatively experimental data within the Gogny [10], Skyrme [7, 11–15], and relativistic frameworks [16–19] (see also a review article Ref. [20]). But until recently, the strength of the tensor force is not well determined and the global effect of the tensor interaction for the nuclei is obscure.

There are two ways to determine the tensor terms in Skyrme EDF. First is to add the tensor terms on top of existing parameter sets and study experimental data of spin–orbit splitting and giant resonances [13–15, 21–24]. The second way is to optimize the central part of Skyrme EDF for a given set of tensor terms. In the optimized process, the parameters of central part of EDF are fitted for a protocol of simultaneous reproduction of nuclear bulk properties such as binding energies and radii of finite nuclei and the empirical characteristics of infinite nuclear matter. For example, Tij EDFs belong to this category [7, 11, 25]. We refer to the first and the second categories as "adiabatic EDF with tensor terms" and "variational EDF with tensor terms," respectively.

By employing empirical excitation energies of Gamow–Teller (GT) and charge-exchange spin–dipole (SD) states in ^{90}Zr and ^{208}Pb and the evolution of energy splitting between proton $h_{11/2}$ and $g_{7/2}$ single-particle orbits along the $Z = 50$ isotopes, our strategy starts firstly from some existing parameter sets and optimizes the tensor terms. Here, we propose optimized tensor interactions for the adiabatic EDFs. We then apply these EDF+optimized tensor terms for the calculations of binding energies of 22 isotopic chains from Ca to Ra to study the contribution of the tensor interactions to the binding energies. Further, we choose a few variational EDFs that have similar tensor terms to the optimized tensor terms of adiabatic EDFs and calculate the evolution of energy splitting between proton $h_{11/2}$ and $g_{7/2}$ states and the binding energies of the 22 isotopic chains. In comparison with the adiabatic EDF and the variational EDF, we explore not only the role of optimized tensor terms for nuclear structure calculations but also the difference between the two approaches.

This paper is organized as follows. In Sect. 2, we briefly describe the formulas of Skyrme EDF that will be used in the calculations. In Sect. 3, the strengths of the tensor terms are optimized by empirical main peak energies of GT and SD transitions in ^{90}Zr and ^{208}Pb and the evolution of energy splitting between proton $h_{11/2}$ and $g_{7/2}$ single-particle orbits along the $Z = 50$ isotopes is examined. Furthermore, the optimized adiabatic and variational EDFs are applied to study the binding energies of 22 isotopic chains by using Hartree–Fock (HF) and Hartree–Fock–Bogolyubov (HFB) models in Sect. 4. The summary is stated in Sect. 5.

2 Formulism

The zero-range two-body tensor force was originally proposed by Skyrme [26, 27]:

$$\begin{aligned} V^T = & \frac{T}{2}\{[(\sigma_1\cdot\mathbf{k}')(\sigma_2\cdot\mathbf{k}') - \frac{1}{3}(\sigma_1\cdot\sigma_2)\mathbf{k}'^2]\delta(\mathbf{r}) \\ & + \delta(\mathbf{r})[(\sigma_1\cdot\mathbf{k})(\sigma_2\cdot\mathbf{k}) - \frac{1}{3}(\sigma_1\cdot\sigma_2)\mathbf{k}^2]\} \\ & + \frac{U}{2}\{(\sigma_1\cdot\mathbf{k}')\delta(\mathbf{r})(\sigma_2\cdot\mathbf{k}) + (\sigma_2\cdot\mathbf{k}')\delta(\mathbf{r})(\sigma_1\cdot k) \\ & - \frac{2}{3}[(\sigma_1\cdot\sigma_2)\mathbf{k}'\cdot\delta(\mathbf{r})\mathbf{k}]\}, \end{aligned} \tag{1}$$

where the operator $\mathbf{k} = (\nabla_1 - \nabla_2)/2\mathrm{i}$ acts on the right and $\mathbf{k}' = -(\nabla_1' - \nabla_2')/2\mathrm{i}$ acts on the left. The parameters T and U denote the strengths of time-even (TE) and time-odd (TO) tensor terms, respectively.

For spherical symmetry, the tensor contributions to the Skyrme EDF are associated with the spin–orbit density J_q :

$$\begin{aligned} J_q = & \frac{1}{4\pi r^3}\sum_{i\in q}(2j_i+1)v_i^2 \\ & \times [j_i(j_i+1) - l_i(l_i+1) - 3/4]R_i^2(r), \end{aligned} \tag{2}$$

where $q = 0(1)$ denotes neutrons (protons), and v_i^2 is the occupation probability of state i, which takes value 1 or 0 for occupied or unoccupied states, respectively, in the closed shell nuclei. The spin–orbit density part of the EDF is given by [7, 28]:

$$\Delta H = \sum_{t=0,1}\frac{1}{2}C_t^J\mathbf{J}_t^2, \tag{3}$$

where the isoscalar and isovector spin–orbit densities are defined by $\mathbf{J}_{t=0} = \mathbf{J}_n + \mathbf{J}_p$ and $\mathbf{J}_{t=1} = \mathbf{J}_n - \mathbf{J}_p$. The coefficients C_t^J receive contributions from both the nonlocal central terms and the tensor terms, namely

$$C_t^J = A_t^J + B_t^J, \tag{4}$$

with

$$A_0^J = \frac{1}{8}t_1\left(\frac{1}{2} - x_1\right) - \frac{1}{8}t_2\left(\frac{1}{2} + x_2\right), \tag{5}$$

$$A_1^J = \frac{1}{16}(t_1 - t_2), \tag{6}$$

$$B_0^J = \frac{5}{48}(T + 3U), \tag{7}$$

$$B_1^J = \frac{5}{48}(U - T). \tag{8}$$

Equation (3) can be represented in the notation used in Ref. [29] as:

$$\Delta H = \frac{1}{2}\alpha\left(J_n^2 + J_p^2\right) + \beta J_n J_p \tag{9}$$

with

$$\alpha = C_0^J + C_1^J, \tag{10}$$

$$\beta = C_0^J - C_1^J. \tag{11}$$

J_q is almost negligible in the spin–orbit saturated nuclei, i.e., in the nuclei with both spin–orbit partners filled.

The contributions of the J^2 tensor terms to the HF spin–orbit potential turn out to be

$$\Delta U_{\mathrm{SO}}^{(q)} = \alpha\frac{J_q}{r} + \beta\frac{J_{q'}}{r}, \tag{12}$$

where $q' = 1 - q$. The contributions of tensor forces to Eq. (12) are

$$\alpha_T = \frac{5}{12}U, \tag{13}$$

$$\beta_T = \frac{5}{24}(T + U). \tag{14}$$

Employing the Skyrme EDF, the self-consistent charge-exchange proton–neutron random phase approximation (*pn*RPA) model is quite an effective method for studying the charge-exchange excitations, such as the GT and charge-exchange SD states. The operators for GT transitions are defined as

$$\hat{O}_{\mathrm{GT}\pm} = \sum_{im} t_{\pm}^i \sigma_m^i, \tag{15}$$

and the spin-dependent charge-exchange SD operators are given by

$$\hat{O}_{\mathrm{SD}\pm}^J = \sum_{iM} t_{\pm}^i r_i (Y_{l=1}^i(\hat{r}) \times \sigma^i)^{JM}, \quad \text{with } J^\pi = 0^-, 1^-, 2^- \tag{16}$$

in terms of the standard isospin operators, $t_\pm = (t_x \pm i t_y)$.

In the EDF+*pn*RPA calculations, the HF equation is solved first in coordinate space with a large reference radius extending up to 20 fm with a mesh step of 0.1 fm. In HF calculations, the single-particle wave functions of the occupied and unoccupied states are obtained by using a harmonic oscillator basis in which the maximum major quantum number $N_{\max} = 10, 12$ for ^{90}Zr and ^{208}Pb, respectively. In the charge-exchange *pn*RPA calculations, all the residual interactions including the central, tensor, and two-body spin–orbit interaction are included to make the calculation fully self-consistent.

3 Constraint for the tensor force

Here, we try to optimize the tensor interaction or choose the existing parameter sets fitted with tensor interaction by using several empirical results. We choose the empirical results from both the shell structure and collective transition of nuclei. For the ground states, we adopt the data of the evolution of energy splitting between $1h_{11/2}$ and $1g_{7/2}$ proton single-particle states along $Z = 50$ isotopes, [8] which is widely used to constrain the tensor interaction [13, 14]. From the collective excitations, it was reported that the GT and SD transitions can also provide a strong constraint for the tensor interaction [21–24].

3.1 Constraint for the tensor force by the adiabatic approach

In this study, we added the tensor forces to the existing Skyrme interactions, SGII and SkO′, which give a better description of the charge-exchange transitions of nuclei. The density functional SGII presented in Ref. [30] was adjusted to provide a reasonable value for the spin–isospin channel of Landau–Migdal parameter $g_0' = 0.503$ with the effective mass 0.79. Bender et al. [31, 32] examined several Skyrme parameter sets and found that the SkO′ is quite promising for studying the GT resonance and β-decay half-lives. The SkO′ interaction gives the Landau–Migdal parameter $g_0' = 0.79$ and the effective mass 0.896.

We calculate the GT and charge-exchange SD excitations in ^{90}Zr and ^{208}Pb by employing SkO′ interaction plus tensor forces in Eq. (1). In the optimizing process, we calculate the centroid energy, which is defined as the ratio between energy-weighted sum rule strength $m(1)$ and non-energy-weighted sum rule strength $m(0)$, i.e., $m(1)/m(0)$ [24]. These centroid energies labeled as E_{th} are then compared with the experimental result E_{exp}. In this study, the excitation energies are calculated with respect to the ground states of the mother nuclei. The difference

$$\Delta E = |E_{\mathrm{th}} - E_{\mathrm{exp}}| \tag{17}$$

is treated as a criterion applied to optimize the tensor parameter sets.

As shown in Fig. 1, the GT and SD transitions are calculated by adopting tensor terms with a sufficiently wide range; $T = (-400 \rightarrow 800)$ MeVfm^5 and $U = (-800 \rightarrow 250)$ MeVfm^5. Within this range, the tensor parameters T and U are constrained by requiring $\Delta E \leq 2.0$ MeV. The allowed range of T varies from approximately 200–700

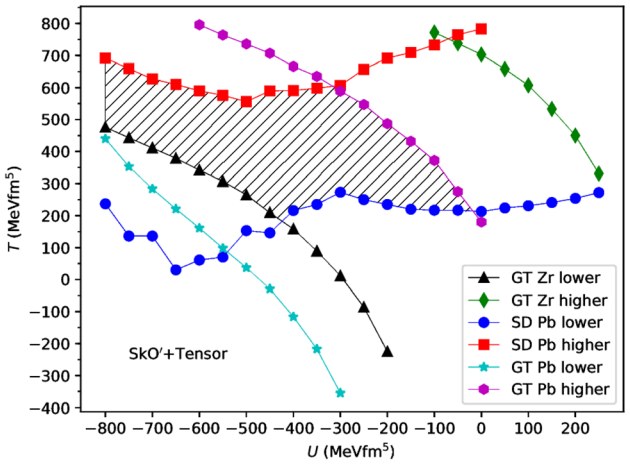

Fig. 1 (Color online) The region of T and U values constrained by the criterion $\Delta E = |E_{\rm th} - E_{\rm exp}| \leq 2.0$ MeV for the GT centroid energies in ^{90}Zr and ^{208}Pb and for the SD 1^- centroid energy in ^{208}Pb

MeVfm^5, which is mainly constrained by the SD 1^- centroid energy in ^{208}Pb. Furthermore, the allowed range of the time-odd tensor strength U is negative varying from approximately -20 to -800 MeVfm^5. The value -800 MeVfm^5 is observed because the RPA equation collapses with U value beyond this border. As the tensor force shifts the GT main peak downward, the line with red squares labeled by "GT Pb higher" implies that when the strengths T and U go beyond this line, the GT main peak energy in ^{208}Pb becomes lower than the $E_{\rm exp} - 2.0 = 17.2$ MeV. Alternately, the line with black triangle labeled by "GT Zr lower" indicates that the strengths of T and U are sufficiently strong to shift the GT main peak energy upward to $E_{\rm exp} + 2.0 = 17.6$ MeV at this border and will exceed the criterion when T and U go beyond this line. The wide allowed range of (T, U) is because the adopted interaction SkO′ has a properly large g_0' value, which makes reproducing the main peak energies of GT and SD more efficient. The optimal values of tensor terms on top of SGII were studied in Ref. [24] in terms of GT and SD excitation energies and are referred to henceforth.

In addition to the main peak energies of GT and SD states, we also study the evolution of spin–orbit splitting of $Z = 50$ isotopes, which is highlighted in the certain tensor force studies [9, 13, 14]. In addition to the central and two-body spin–orbit terms of Skyrme interaction, the tensor terms contribute to the spin–orbit splitting which modifies the SPE remarkably [29]. Thus, the energy splitting along an isotopic or isotonic chain may produce strong constraint for the strengths of tensor terms. Hence, the proton SPE splitting between $1h_{11/2}$ and $1g_{7/2}$ of Sn isotopes with N varying from 56–82 has been calculated to further constrain the strength of tensor terms.

In our calculation, the Hartree–Fock–Bogolyubov (HFB) model described in Ref. [33, 34] was applied, solving the Skyrme HFB equations in coordinate space under the spherical symmetry. The zero-range surface pairing interaction is used:

$$V = V_0\left(1 - \frac{\rho\left(\frac{\mathbf{r}_1+\mathbf{r}_2}{2}\right)}{\rho_0}\right)\delta(\mathbf{r}_1 - \mathbf{r}_2), \tag{18}$$

where the density parameter ρ_0 is set to be 0.16 fm^{-3} and the strength parameter V_0 is determined to reproduce the empirical value of neutron pairing gap calculated by the three-point index $\Delta(3) = (B(N,Z) - 2B(N+1,Z) + B(N+2,Z))/2$.

The evolution of proton SPE splitting between $1h_{11/2}$ and $1g_{7/2}$ states is calculated in HFB model adopting the Skyrme EDFs with and without tensor interactions and shown in Fig. 2. In the calculations, SGII and SkO′ are adopted. The strengths of tensor interactions are set to be $(T, U) = (500, -320)$ and $(500, -480)$, respectively, for SkO′ and SGII. It is observed that the presently optimized density functionals with tensor terms SkO′+(500, -320) and SGII+ (500, -480) reproduce the empirical data.

For a quantitative study of optimizations of tensor interactions, we examine the following criterion for the energy difference $\delta = \varepsilon_{1h11/2} - \varepsilon_{1g7/2}$, i.e., the root mean squared deviation (RMSD) between calculated and empirical energy differences:

$$\mathrm{RMSD}(|\delta_{\rm th} - \delta_{\rm exp}|) = \sqrt{\frac{1}{N_D}\sum_N |\delta_{\rm th}(N) - \delta_{\rm exp}(N)|^2} \tag{19}$$

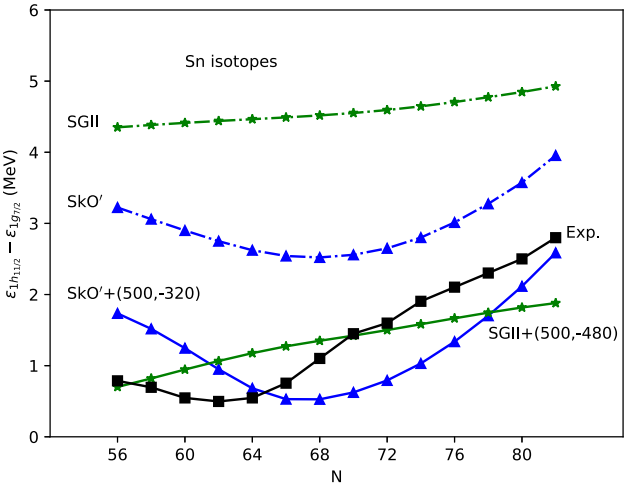

Fig. 2 (Color online) The energy differences between $1h_{11/2}$ and $1g_{7/2}$ proton single-particle states along Sn isotopes with $N = 56-82$. The calculations are performed by implying SkO′ without (labeled by SkO′) and with (labeled by SkO′+(T, U)) tensor force, and SGII without and with tensor terms. The experimental data are taken from Ref. [8]

where N_D is the number of data points. For the calculated results in Fig. 2, RMSD values are 1.67, 0.65, 3.24, and 0.47 for SkO′, SkO′+tensor, SGII, and SGII+tensor, respectively. To constrain T and U values, we set RMSD to be less than 1 MeV. The optimized parameter region for T and U is shown in Fig. 3 for SkO′ and Fig. 4 for SGII, respectively. As observed in the figures, the isotope dependence of SPE splittings provides a strict constraint for the strength of time-odd tensor term U. The range of U is further constrained to be from -150 to -450 MeVfm^5 and from -350 to -550 MeVfm^5 for SkO′ and SGII, respectively. The tensor interactions within this range produce attractive effects on the binding energy of ground state, which can be qualitatively understood from Eqs. (9), (13), and (14).

3.2 The variational EDFs with the tensor terms

It was reported in Ref. [24] that some variational EDFs T21, T32, T43, and T54 in Tij family can well reproduce the GT and SD empirical data in ^{90}Zr and ^{208}Pb. The evolution of proton SPE splitting between $1h_{11/2}$ and $1g_{7/2}$ states is also calculated in HFB model adopting the four parameter sets from Tij family and is shown in Fig. 5. For the calculated results in Fig. 5, RMSD values for T21 are 1.08 MeV, while they are 1.52, 1.81, and 2.17 MeV for T32, T43, and T54, respectively. While the agreement of Tij family is not as efficient as those of the adiabatic EDFs, SkO′+tensor, and SGII+tensor, it should be noticed that the best T21 among Tij family has similar tensor terms as the two adiabatic EDFs as listed in Table 1. According to

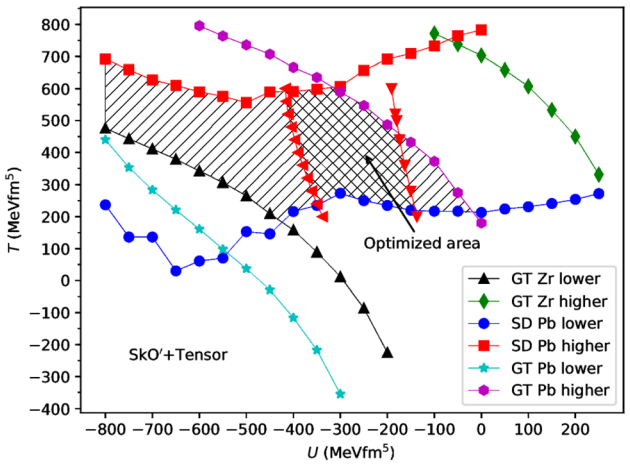

Fig. 3 (Color online) The region of T and U values optimized by the $1h_{11/2}$ and $1g_{7/2}$ proton single-particle energy differences along Sn isotopes with N from 56–82. The area constrained by GT and SD states shown in Fig. 1 is further optimized to be the meshed region, indicated by the optimized area. The criterion for the constrain is set to be the RMSD value in Eq. (19) to be smaller than 1 MeV

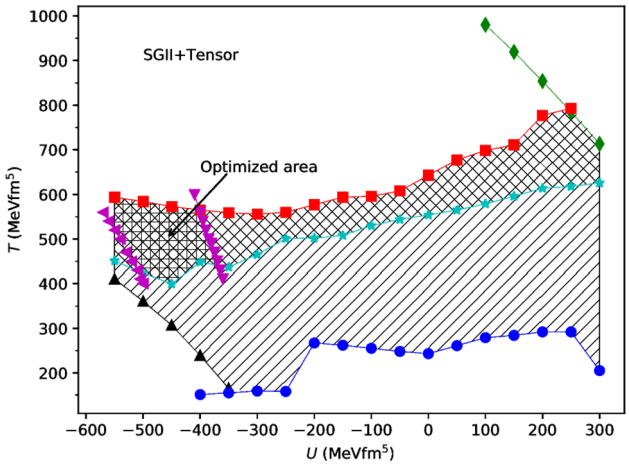

Fig. 4 (Color online) The same as Fig. 3, but for SGII. See the text for more details

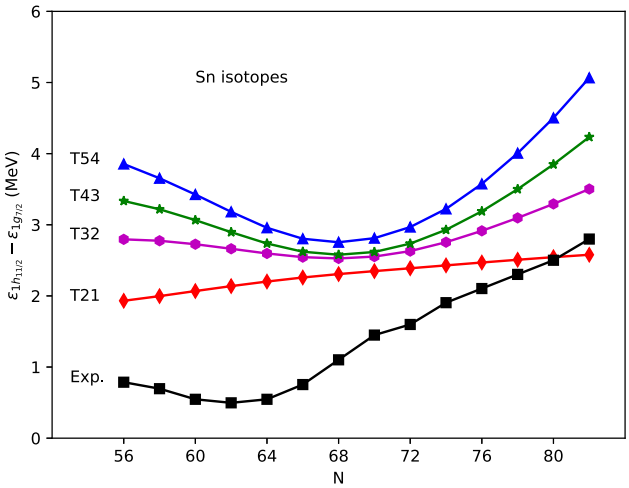

Fig. 5 (Color online) Same as in Fig. 2, but calculated with T21, T32, T43, and T54 parameter sets

Eq. (3), the three sets of EDFs with tensor parameters, SkO′+, SGII+, and T21 will produce an attractive effect for the binding energy as the α_T values are negative and larger than the corresponding positive β_T values.

4 The optimized tensor terms on the binding energies

Nuclear binding energy, i.e., the nuclear mass, is important for the study of nuclear reactions such as the r-process synthesis of nuclei [35] as well as the β-delayed multi-nucleon emission. Furthermore, it is of great importance for the studies of the superheavy nuclei and the dripline nuclei [36, 37]. In recent years, many efforts have been devoted to accurately measuring the nuclear mass of unstable nuclei [38–42]. Theoretically, there are some

Table 1 Time-even and time-odd tensor parameters T and U in Eq. (1)

	SkO′+	SGII+	T21	T32	T43	T54
T (MeVfm^5)	500.00	500.00	476.95	613.06	590.60	727.35
U (MeVfm^5)	− 320.00	− 480.00	− 369.36	− 231.53	− 147.48	− 8.36
α_T (MeVfm^5)	− 133.33	− 162.5	− 153.90	− 96.47	− 61.45	− 3.48
β_T (MeVfm^5)	37.5	4.17	22.42	79.48	93.32	147.79

The tensor contributions α_T and β_T (MeVfm^5) to the spin–orbit potential (12) are given by Eqs. (13) and (14)

successful macroscopic and microscopic models of nuclear mass [43–53], which can provide accurate mass tables, but the tensor interaction was not included in these models. A Skyrme EDF UNEDF2 [54], which includes the tensor terms and optimizes both the ground state properties and shell structure, provides reasonable binding energies of heavy nuclei, in which the tensor interaction also produces an attractive effect. In this section, we apply the optimized Skyrme EDFs SKO′ and T21 without and with tensor terms for the binding energies of 22 isotopic chains from Ca to Ra. Although some nuclei in the study might be deformed, we adopt the HFB model with spherical symmetry. Thus, the nuclei studied are selected to be spherical or at most weakly deformed with the deformation parameter $\beta_2 < 0.3$.

The binding energies of the Sn isotopes are calculated with SkO′, SGII, and T21 with and without tensor terms listed in Table 1. The differences of the binding energies between the theoretical and experimental values are illustrated in Fig. 6. As shown in Fig. 6, both the SkO′ and T21 without tensor terms give less bound of the order of approximately 5–10 MeV than the experimental data. SGII gives the overbindings for all Sn isotopes, and SGII+(500, -480) does not contribute to this feature of binding energies. With the tensor interaction included in the calculations, both SkO′+tensor and T21 can reproduce the experimental data within a few MeV difference for all the Sn isotopes.

We apply further SkO′ and T21 with and without tensor interaction for the binding energies of 22 isotopic chains of spherical and weakly deformed medium-heavy and heavy nuclei. The difference between the calculated binding energies and the corresponding experimental values [55] is shown in Figs. 7 and 8 for SKO′ and T21, respectively. Inclusion of the tensor interaction in both SKO′ and T21

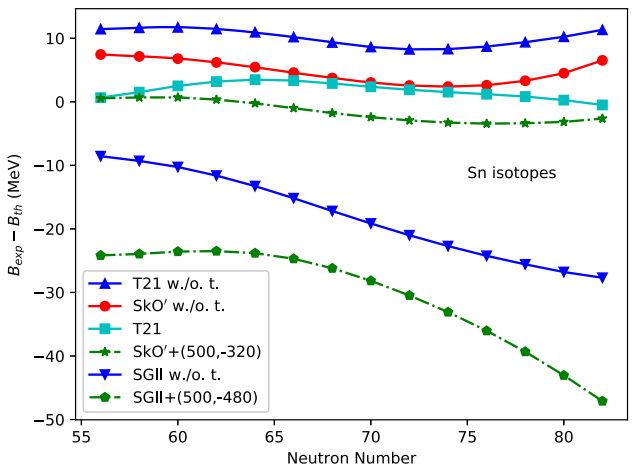

Fig. 6 (Color online) Difference of binding energies between theoretical and experimental values for Sn isotopes. The HFB calculations are performed by using the EDFs SkO′, SGII, and T21 with and without tensor terms. See text for more details

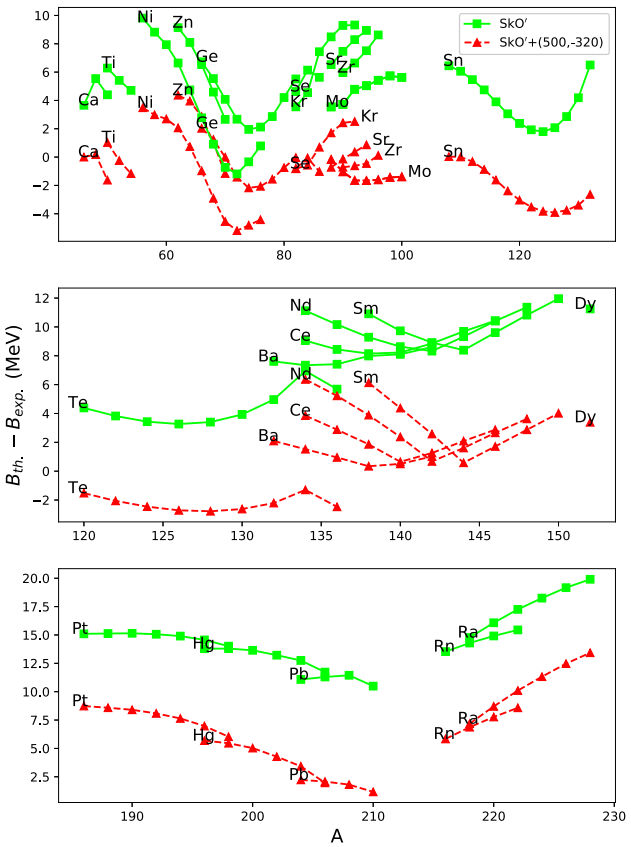

Fig. 7 (Color online) Difference of binding energies between theoretical and experimental values for various isotopes. Calculated results are obtained by using SkO′ without (green squares) and with tensor force (red triangles). The adopted tensor parameters (T, U) are (500, − 320). The experimental values are taken from Ref. [55]. Each line expresses one isotopic chain

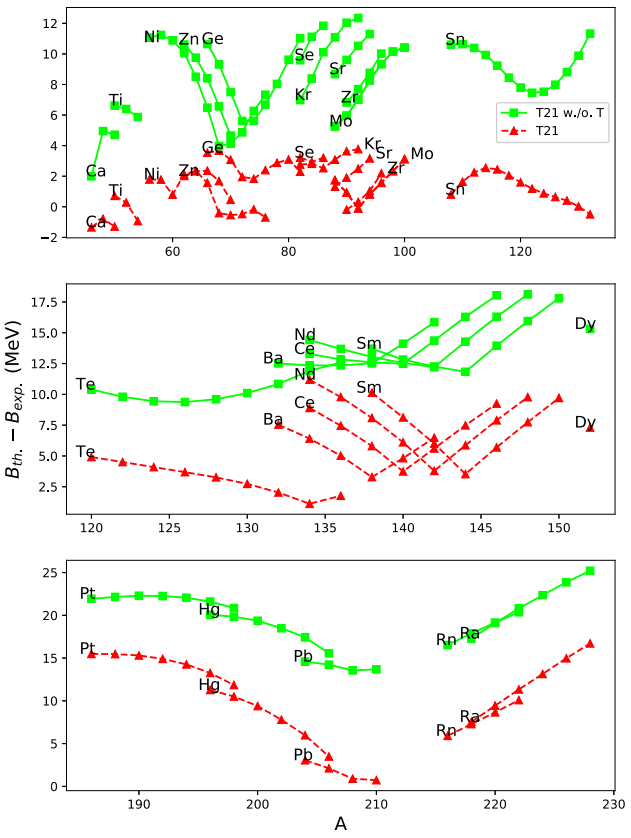

Fig. 8 (Color online) Same as Fig. 7, but calculated with T21 with and without the tensor interaction

increases the total binding energies systematically and improves the results.

The RMSD for the calculated binding energies with respect to the experimental values is calculated as follows:

$$\mathrm{RMSD}(B) = \sqrt{\frac{1}{N_{\mathrm{tot}}}\sum_{i=1}^{N_{\mathrm{tot}}}\left(B(N_i,Z_i)_{\mathrm{th.}} - B(N_i,Z_i)_{\mathrm{exp.}}\right)^2}, \tag{20}$$

where N_{tot} is the number of nuclei. For SKO′, the RMSD(B) for all of the calculated nuclei shown in Fig. 7 is 8.97 MeV and 3.99 MeV for SkO′ without and with tensor terms, respectively. For T21, as shown in Fig. 8, the RMSD(B) is approximately 13 MeV and 6.2 MeV without and with tensor interaction. The two EDFs with tensor terms give good global agreements of the binding energies, and although the two EDFs are optimized by different strategic approaches, the tensor contributions to the binding energies are quite similar, i.e., approximately 5 MeV for SKO′+tensor and 6.8 MeV for T21 .

5 Summary

We adopted the GT and charge-exchange SD centroid energies and the evolution of proton SPE difference between $1h_{11/2}$ and $1g_{7/2}$ orbits of Sn isotopes as the constraints to choose appropriate parameter sets of tensor terms. We first implemented the adiabatic approach and optimized the tensor terms T and U on top of existing parameter sets SkO′ and SGII. The time-even tensor parameter T is well controlled by the energies of GT and SD giant resonances. Further, a strong constraint on the time-odd tensor term U comes mainly from the SPE splitting between proton $h_{11/2}$ and $g_{7/2}$ orbits along the Z=50 isotopes. For the adiabatic EDFs, the constraints provide a small region of the (T, U) parameters both for SGII and SkO′; $T = (400-600)\mathrm{MeVfm}^5$ and $U = (-350\,\mathrm{to}\,-550)\mathrm{MeVfm}^5$ for SGII and T =(250 to 600)MeVfm^5 and $U = (-150\,\mathrm{to}\,-450)\mathrm{MeVfm}^5$ for SkO′. The optimized adiabatic parameter sets suggest T21 EDF as the best candidate for nuclear structure calculations among Tij family, as T21 has very similar tensor terms to the adiabatic EDFs, SkO′+tensor, and SGII+tensor. Because of these constraints, the tensor interaction provides an attractive effect for the binding energies of nuclei, which is consistent with the primary purpose of introducing tensor interaction to make deuteron and light nuclei bound [56, 57].

Qualitatively, the Skyrme interaction with tensor terms, $\alpha_T < 0$ and $\beta_T > 0$, acts similar to the realistic interactions in the proton–neutron channel and the isospin dependence of spin–orbit coupling [12, 20, 58]. The EDFs SkO′ and T21 with and without the tensor terms are further applied for the study of binding energies of 22 isotopic chains from Ca to Ra. Though the SkO′+tensor and T21 EDFs are obtained in different methodologies, i.e., the central terms are optimized without and with tensor terms, the RMSD deviation of binding energies is approximately 3.99 MeV and 6.2 MeV, respectively. Furthermore, the similar average contributions of the tensor terms are evaluated for the binding energies to be approximately 5 and 6.8 MeV for SKO′ and T21, respectively, which originated from a negative strength of time-odd tensor term U. Further, we will develop a systematic study of optimized variational EDFs based on the tensor terms obtained by the present adiabatic study of EDF+tensor terms. This study will provide more reliable estimates of β-decay half-lives and neutron capture rates of r-process nucleosynthesis.

References

1. D. Vautherin, D.M. Brink, Hartree–Fock calculations with Skyrme's interaction. I. Spherical nuclei. Phys. Rev. C **5**, 626 (1972). https://doi.org/10.1103/PhysRevC.5.626
2. J. Decharge, D. Gogny, Hartree–Fock–Bogolyubov calculations with the $D1$ effective interaction on spherical nuclei. Phys. Rev. C **21**, 1568 (1980). https://doi.org/10.1103/PhysRevC.21.1568
3. M. Bender, P.-H. Heenen, Self-consistent mean-field models for nuclear structure. Rev. Mod. Phys. **75**, 121 (2003). https://doi.org/10.1103/RevModPhys.75.121
4. J. Meng (ed.), *Relativistic Density Functional for Nuclear Structure* (World Scientific, Singapore, 2016). https://doi.org/10.1142/987
5. G.E. Brown, T.T.S. Kuo, J.W. Holt et al., *The Nucleon Nucleon Interaction and the Nuclear Many-Body Problem* (World Scientific, Singapore, 2010)
6. I.R. Afnan, D.M. Clement, F.J.D. Serduke, The tensor force in nuclear saturation. Nucl. Phys. A **170**, 625 (1971). https://doi.org/10.1016/0375-9474(71)90242-9
7. T. Lesinski, M. Bender, K. Bennaceur et al., Tensor part of the Skyrme energy density functional: spherical nuclei. Phys. Rev. C **76**, 014312 (2007). https://doi.org/10.1103/PhysRevC.76.014312
8. J.P. Schiffer, S.J. Freeman, J.A. Caggiano et al., Is the nuclear spin–orbit interaction changing with neutron excess? Phys. Rev. Lett. **92**, 162501 (2004). https://doi.org/10.1103/PhysRevLett.92.162501
9. T. Otsuka, T. Suzuki, R. Fujimoto et al., Evolution of nuclear shells due to the tensor force. Phys. Rev. Lett. **95**, 232502 (2005). https://doi.org/10.1103/PhysRevLett.95.232502
10. T. Otsuka, T. Matsuo, D. Abe, Mean field with tensor force and shell structure of exotic nuclei. Phys. Rev. Lett. **97**, 162501 (2006). https://doi.org/10.1103/PhysRevLett.97.162501
11. M. Bender, K. Bennaceur, T. Duguet et al., Tensor part of the Skyrme energy density functional. II. Deformation properties of magic and semi-magic nuclei. Phys. Rev. C **80**, 064302 (2009). https://doi.org/10.1103/PhysRevC.80.064302
12. B.A. Brown, T. Duguet, T. Otsuka et al., Tensor interaction contributions to single-particle energies. Phys. Rev. C **74**, 061303(R) (2006). https://doi.org/10.1103/PhysRevC.74.061303
13. G. Colò, H. Sagawa, S. Fracasso et al., Spin–orbit splitting and the tensor component of the Skyrme interaction. Phys. Lett. B **646**, 227 (2007). https://doi.org/10.1016/j.physletb.2007.01.033
14. D.M. Brink, Fl Stancu, Evolution of nuclear shells with the Skyrme density dependent interaction. Phys. Rev. C **75**, 064311 (2007). https://doi.org/10.1103/PhysRevC.75.064311
15. D.M. Brink, Fl Stancu, Skyrme density functional description of the double magic ^{78}Ni nucleus. Phys. Rev. C **97**, 064304 (2018). https://doi.org/10.1103/PhysRevC.97.064304
16. W. Long, H. Sagawa, J. Meng et al., Evolution of nuclear shell structure due to the pion exchange potential. Europhys. Lett. **82**, 12001 (2008). https://doi.org/10.1209/0295-5075/82/12001
17. L.J. Jiang, S. Yang, B.Y. Sun et al., Nuclear tensor interaction in a covariant energy density functional. Phys. Rev. C **91**, 034326 (2015). https://doi.org/10.1103/PhysRevC.91.034326
18. Y.-Y. Zong, B.-Y. Sun, Relativistic interpretation of the nature of the nuclear tensor force. Chin. Phys. C **42**, 024101 (2018). https://doi.org/10.1088/1674-1137/42/2/024101
19. Z. Wang, Q. Zhao, H. Liang et al., Quantitative analysis of tensor effects in the relativistic Hartree–Fock theory. Phys. Rev. C **98**, 034313 (2018). https://doi.org/10.1103/PhysRevC.98.034313
20. H. Sagawa, G. Colò, Tensor interaction in mean-field and density functional theory approaches to nuclear structure. Prog. Part. Nucl. Phys. **76**, 76 (2014). https://doi.org/10.1016/j.ppnp.2014.01.006
21. C.L. Bai, H. Sagawa, H.Q. Zhang et al., Effect of tensor correlations on Gamow–Teller states in Zr-90 and Pb-208. Phys. Lett. B **675**, 28 (2009). https://doi.org/10.1016/j.physletb.2009.03.077
22. C.L. Bai, H.Q. Zhang, X.Z. Zhang et al., Quenching of Gamow–Teller strength due to tensor correlations in ^{90}Zr and ^{208}Pb. Phys. Rev. C **79**, 041301(R) (2009). https://doi.org/10.1103/PhysRevC.79.041301
23. C.L. Bai, H.Q. Zhang, H. Sagawa et al., Effect of the tensor force on the charge exchange spin–dipole excitations of ^{208}Pb. Phys. Rev. Lett. **105**, 072501 (2010). https://doi.org/10.1103/PhysRevLett.105.072501
24. C.L. Bai, H.Q. Zhang, H. Sagawa et al., Spin–isospin excitations as quantitative constraints for the tensor force. Phys. Rev. C **83**, 054316 (2011). https://doi.org/10.1103/PhysRevC.83.054316
25. S.H. Shen, G. Colò, X. Roca-Maza, Skyrme functional with tensor terms from *ab initio* calculations of neutron-proton drops. Phys. Rev. C **99**, 034322 (2019). https://doi.org/10.1103/PhysRevC.99.034322
26. T.H.R. Skyrme, The effective nuclear potential. Nucl. Phys. **9**, 615 (1959). https://doi.org/10.1016/0029-5582(58)90345-6
27. T.H.R. Skyrme, CVII. The nuclear surface. Philos. Mag **1**, 1043 (1956). https://doi.org/10.1080/14786435608238186
28. E. Perlińska, S.G. Rohoziński, J. Dobaczewski, W. Nazarewicz, Local density approximation for proton-neutron pairing correlations: formalism. Phys. Rev. C **69**, 014316 (2004). https://doi.org/10.1103/PhysRevC.69.014316
29. Fl Stancu, D.M. Brink, H. Flocard, The tensor part of Skyrme's interaction. Phys. Lett. B **68**, 108 (1977). https://doi.org/10.1016/0370-2693(77)90178-2
30. N.V. Giai, H. Sagawa, Spin–isospin and pairing properties of modified Skyrme interactions. Phys. Lett. B **106**, 379 (1981). https://doi.org/10.1016/0370-2693(81)90646-8
31. J. Engel, M. Bender, J. Dobaczewski et al., β decay rates of r-process waiting-point nuclei in a self-consistent approach. Phys. Rev. C **60**, 014302 (1999). https://doi.org/10.1103/PhysRevC.60.014302
32. M. Bender, J. Dobaczewski, J. Engel et al., Gamow–Teller strength and the spin–isospin coupling constants of the Skyrme energy functional. Phys. Rev. C **65**, 054322 (2002). https://doi.org/10.1103/PhysRevC.65.054322
33. J. Dobaczewski, H. Flocard, J. Treiner, Hartree–Fock–Bogolyubov descriptions of nuclei near the neutrino dripline. Nucl. Phys. A **422**, 103 (1984). https://doi.org/10.1016/0375-9474(84)90433-0
34. K. Bennaceur, J. Dobaczewski, Coordinate-space solution of the Skyrme–Hartree–Fock–Bogolyubov equations within spherical symmetry. The Program HFBRAD (v1.00). Comput. Phys. Commun. **168**, 96 (2005). https://doi.org/10.1016/j.cpc.2005.02.002
35. B.H. Sun, YuA Litvinov, I. Tanihata et al., Toward precision mass measurements of neutron-rich nuclei relevant to r-process nucleosynthesis. Front. Phys. **10**, 102102 (2015). https://doi.org/10.1007/s11467-015-0503-z
36. S.K. Patra, C.L. Wu, C.R. Praharaj et al., A systematic study of superheavy nuclei for $Z = 114$ and beyond using the relativistic mean field approach. Nucl. Phys. A **651**, 117 (1999). https://doi.org/10.1016/S0375-9474(99)00129-3
37. T.K. Dong, Z.Z. Ren, Improved version of a binding energy formula for heavy and superheavy nuclei with $Z \geq 90$ and $N \geq 140$. Phys. Rev. C **77**, 064310 (2008). https://doi.org/10.1103/PhysRevC.77.064310
38. Y.H. Zhang, Y.A. Litvinov, T. Uesaka et al., Storage ring mass spectrometry for nuclear structure and astrophysics research. Phys. Scr. **91**, 073002 (2016). https://doi.org/10.1088/0031-8949/91/7/073002

39. H.S. Xu, Y.H. Zhang, Y.A. Litvinov, Accurate mass measurements of exotic nuclei with the CSRe in Lanzhou. Int. J. Mass Spectrom. **349–350**, 162–171 (2013). https://doi.org/10.1016/j.ijms.2013.04.029
40. M.Z. Sun, X.H. Zhou, M. Wang et al., Precision mass measurements of short-lived nuclides at HIRFL-CSR in Lanzhou. Front. Phys. **13**(6), 132112 (2018). https://doi.org/10.1007/s11467-018-0844-5
41. M. Mougeot, D. Atanasov, K. Blaum et al., Precision mass measurements of $^{58-63}$Cr: Nuclear collectivity towards the $N = 40$ island of inversion. Phys. Rev. Lett. **120**, 232501 (2018). https://doi.org/10.1103/PhysRevLett.120.232501
42. J.H. Liu, Z. Ge, Q. Wang et al., Electrostatic-lenses position-sensitive TOF MCP detector for beam diagnostics and new scheme for mass measurements at HIAF. Nucl. Sci. Technol. **30**, 152 (2019). https://doi.org/10.1007/s41365-019-0676-1
43. C.F. Weizsäcker, Zur Theorie der Kernmassen. Z. Phys. **96**, 431 (1935). https://doi.org/10.1007/BF01337700
44. R.F. Bethe, Physics A. Nuclear, Stationary states of nuclei. Rev. Mod. Phys. **8**, 82 (1936). https://doi.org/10.1103/RevModPhys.8.82
45. P. Möller, J.R. Nix, W.D. Myers et al., Nuclear ground state masses and deformations. At. Data Nucl. Data Tables **59**, 185 (1995). https://doi.org/10.1006/adnd.1995.1002
46. N. Wang, M. Lin, Nuclear mass predictions with a radial basis function approach. Phys. Rev. C **84**, 051303(R) (2011). https://doi.org/10.1103/PhysRevC.84.051303
47. M. Liu, N. Wang, Y.G. Deng et al., Further improvements on a global nuclear mass model. Phys. Rev. C **84**, 014333 (2011). https://doi.org/10.1103/PhysRevC.84.014333
48. N. Wang, M. Liu, X.Z. Wu, Modification of nuclear mass formula by considering isospin effects. Phys. Rev. C **81**, 044322 (2010). https://doi.org/10.1103/PhysRevC.81.044322
49. N. Wang, M. Liu, X.Z. Wu et al., Surface diffuseness correction in global mass formula. Phys. Lett. B **734**, 215 (2014). https://doi.org/10.1016/j.physletb.2014.05.049
50. W.J. Huang, G. Audi, M. Wang et al., The AME2016 atomic mass evaluation (I). Evaluation of input data; and adjustment procedures. Chin. Phys. C **41**, 030002 (2017). https://doi.org/10.1088/1674-1137/41/3/030002
51. M. Wang, G. Audi, F.G. Kondev et al., The AME2016 atomic mass evaluation (II). Tables, graphs and references. Chin. Phys. C **41**, 030003 (2017). https://doi.org/10.1088/1674-1137/41/3/030003
52. S. Goriely, N. Chamel, J.M. Pearson, Further explorations of Skyrme–Hartree–Fock–Bogoliubov mass formulas. XIII. The 2012 atomic mass evaluation and the symmetry coefficient. Phys. Rev. C **88**, 024308 (2013). https://doi.org/10.1103/PhysRevC.88.024308
53. S. Goriely, N. Chamel, J.M. Pearson, Further explorations of Skyrme–Hartree–Fock–Bogoliubov mass formulas. XVI. Inclusion of self-energy effects in pairing. Phys. Rev. C **93**, 034337 (2016). https://doi.org/10.1103/PhysRevC.93.034337
54. M. Kortelainen, J. McDonnell, W. Nazarewicz et al., Nuclear energy density optimization: shell structure. Phys. Rev. C **89**, 054314 (2014). https://doi.org/10.1103/PhysRevC.89.054314
55. G. Audi, A.H. Wapstra, C. Thibault, The Ame2003 atomic mass evaluation (II). Tables, graphs and references. Nucl. Phys. A **729**, 337 (2003). https://doi.org/10.1016/j.nuclphysa.2003.11.003
56. W. Rarita, J. Schwinger, On the neutron-proton interaction. Phys. Rev. **59**, 436 (1941). https://doi.org/10.1103/PhysRev.59.436
57. H. Feshbach, W. Rarita, Tensor forces and the triton binding energy. Phys. Rev. **75**, 1384 (1949). https://doi.org/10.1103/PhysRev.75.1384
58. J.W. Negele, D. Vautherin, Density-matrix expansion for an effective nuclear hamiltonian. Phys. Rev. C **5**, 1472 (1972). https://doi.org/10.1103/PhysRevC.5.1472